Robotica (2021), **39**, pp. 2172–2192
doi:10.1017/S0263574721000242

CAMBRIDGE
UNIVERSITY PRESS

RESEARCH ARTICLE

Stiffness modulation of a cable-driven leg exoskeleton for effective human–robot interaction

N. S. S. Sanjeevi and Vineet Vashista*

Human Centered Robotics Lab, IIT Gandhinagar, Ahmedabad, India
E-mail: nakka.suryasatyasanjeevi@iitgn.ac.in
*Corresponding author. Email: vineet.vashista@iitgn.ac.in

Received: 15 January 2020; **Revised:** 10 February 2021; **Accepted:** 12 February 2021; **First published online:** 28 April 2021

Keywords: Human–Robot interaction, Gait rehabilitation; Exoskeleton, Cable-driven robots, Stiffness modulation

Abstract

With the widespread development of leg exoskeletons to provide external force-based repetitive training for gait rehabilitation, the prospect of undesired movement adaptation due to applied forces and imposed constraints require adequate investigation. A cable-driven leg exoskeleton, CDLE, presents a lightweight, flexible, and redundantly actuated architecture that enables the possibility of system parameters modulation to alter human–robot interaction while applying the desired forces. In this work, multi-joint stiffness performance of CDLE is formulated to systematically analyze human–CDLE interaction. Further, potential alterations in CDLE architecture are presented to tune human–CDLE interaction that favors the desired human leg movement during a gait rehabilitation paradigm.

1. Introduction

Walking enables a human to accomplish many different activities of daily living. Notably, human walking is a mechanically complex mode of locomotion, yet it is the most convenient way to travel short distances. During walking, a person retains one leg in contact with the ground while advancing the body forward through the swing of the other leg. Alternate and repetitive execution of such leg movements with a period of foot-to-foot transition enables a symmetric and energy-efficient walking pattern. Incidentally, any occurrence of a neuro-musculoskeletal disorder can significantly affect human walking performance.

Neurological disorders, such as stroke and spinal cord injury, are prevalent worldwide and have been reported to be the major cause of long-term walking disability [1]. These disorders affect an individual's ability to perceive sensory feedback and to coordinate the muscle actuation to generate the muscular force required to apply lower limb joint torques during different phases of walking. This results in significant gait abnormalities, which are typically characterized by slow walking speed, gait asymmetry, poor balance and fall control, and higher metabolic cost [2].

To improve the functional walking of individuals with neurological disorders, several gait rehabilitation paradigms have been proposed in the literature to provide repetitive practice sessions to train the affected leg [3, 4, 5, 6]. In conventional practices [7], a patient walks on a treadmill with support to prevent falls and in some cases to provide partial body weight support. These practices require multiple physical therapists, are in general highly labor-intensive, and lack quantitative feedback. In the last two decades, many robotic leg exoskeletons have been developed for gait rehabilitation [8, 9, 10, 11] for their advantages in providing controlled repetitive motion, better quantification of motor recovery, and reduced labor need [9]. In addition, these devices can be programmed and controlled to implement novel gait rehabilitation methodologies.

The design goal of these devices is to assist the leg and ensure it to be moving along the desired foot trajectory [12, 13]. Typically, the leg exoskeletons are modeled as a serial-chain manipulator that mainly assists joint motion during the swing phase of walking. In most cases, external forces are applied on the thigh and shank segments to generate the sagittal plane hip and knee joint torque to minimize the error in following the desired foot trajectory. Studies with these devices report adaptations in the human walking pattern [14, 15], which implies some level of adjustments by the human musculoskeletal system when external forces are applied on the leg. Thus, the way external forces are applied is an important component of a leg exoskeleton-based rehabilitation paradigm. Further, the studies on the role of mass/inertia and joint mobility constraints, which arise due to the use of rigid links for actuation, on the human walking adaptation highlight the importance of design and architecture of a robotic exoskeleton [16, 17]. Essentially, the effectiveness of a robotic-based gait rehabilitation paradigm depends on the ensued physical human–robot interaction.

Consequently, with the purpose of improving human–robot interaction, several modalities through design alterations, addition of sensors, and control strategies have been implemented in the works on exoskeletons [18, 19, 20, 21, 22, 23]. In general, from rigid-link exoskeletons design aspect, the physical interaction with humans is improved primarily by utilizing lightweight components and by altering actuator transmission compliance that promotes backdrivability, shock tolerance, and torque fidelity. Further, control strategies based on human motion, such as force, impedance, and admittance control, to compute the applied joint torques have been implemented in exoskeletons. Accordingly, series elastic actuators for torque generation and force–torque sensors at the human–exoskeleton interfaces are employed to improve exoskeleton transparency and to present an overall exoskeleton compliance to the user. Additionally, understandings derived from human physiological sensors, such as Electromyography (EMG) and Electroencephalogram (EEG) are being incorporated at the high-level controller mainly to control the level of assistance in accordance with human motion intent.

Among the works on leg exoskeletons [13, 24, 25, 26], cable-driven-based architectures are also being used for movement rehabilitation. Owing to the use of cables, these systems provide inherent advantages of being lightweight, flexible, and ease of altering cable routing. However, unlike a rigid link, a cable can only apply a pulling force on a body and can only be used for unidirectional force applications [27, 28]. This makes a cable-driven leg exoskeleton (CDLE) analogous to the human musculoskeletal structure as it requires redundantly actuated cables to control the system. Notably, the redundancy in actuation leads to multiple solution conditions, which implies that a redundantly actuated CDLE can apply the desired set of joint torques even when the system parameters are varied. Consequently, the control of CDLE has been approached differently from rigid-link exoskeletons [24, 25, 26, 29]. In particular, either position and velocity controls, which require solution to a complex problem of inverse kinematics, or force control, where numerical methods are typically used to plan cable tensions, have been implemented.

The literature on the cable-driven industrial robotic systems [30] reports a significant variation in the robot's stiffness performance with alterations in actuator positions and cable attachment locations. In the context of CDLE, such changes in the system architecture that alter its stiffness performance imply modulation of physical interaction between the CDLE and human. Thus, in addition to the use of actuator compliance, the flexibility in architecture modulation to augment the multi-joint stiffness of a CDLE can enable the possibility of favorably tuning the human–robot interaction. As humans adapt their walking pattern differently when subjected to different external conditions [31], having a CDLE joint stiffness that incorporates human anatomical joint stiffness aspects [32, 33] can be used to promote the effectiveness of a gait rehabilitation paradigm. Accordingly, there is a need to understand the human–CDLE interaction and to identify the effect of varying CDLE parameters.

The main focus of this work is to formulate the multi-joint stiffness characteristics of a CDLE as a measure to model human–CDLE interaction during a gait cycle. Further, the dependency of CDLE stiffness performance on system architecture and parameters is analyzed. The potential of a CDLE in achieving a diverse stiffness characteristics by appropriately tuning the system parameters is validated experimentally. The stiffness analysis is performed for a redundant CDLE to apply hip and knee joints

https://doi.org/10.1017/S0263574721000242 Published online by Cambridge University Press

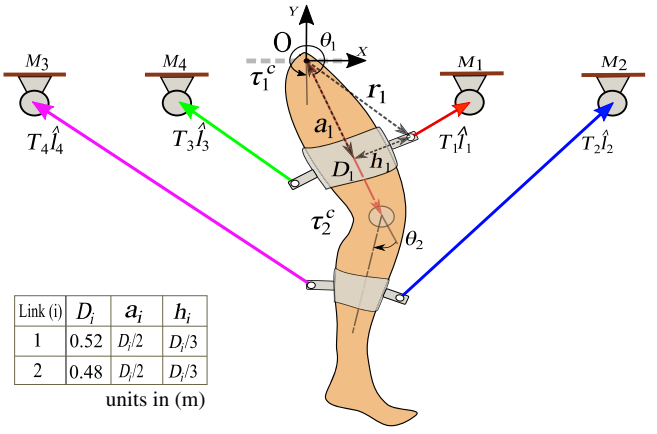

Figure 1. *Schematic of a general CDLE. T_i and l_i represent cable tension and length of the i^{th} cable, respectively. D_i, r_i, and h_i represent segment lengths, cable attachment points, and offset position on each segment. τ_i denotes the joint torque and M_i represents the motor positions w.r.t O .*

torque equivalent to 30% of the corresponding anatomical values over a gait cycle using the human gait kinematics data from literature [34]. The effect of system parameters, including cable tension distribution, motor positions, cable routing, and cable stiffness, on multi-joint stiffness has been discussed. Finally, an experimental setup of a cable-driven manipulator is developed to compute the stiffness values theoretically for two different architectures at different configurations.

2. Cable-driven leg exoskeleton

Leg exoskeletons are developed to provide external torque assistance at the hip and knee joints during walking. As human anatomical architecture comprises of thigh, shank, and foot segments connected in series, a typical leg exoskeleton is given a serial-chain manipulator architecture, where externally actuated elements are attached to the segments. In this work, we considered a leg exoskeleton driven by cables in which external forces on the leg segments are applied through motor-actuated cables. Figure 1 shows a schematic of a general CDLE architecture. Sagittal plane leg model with hip and knee joints flexion-extension motion is considered for the analysis. It has been established that to control a n degrees of freedom (DOFs) system, at least $m = n + 1$ cables are needed [27, 28]. This is because a cable can only be pulled but not pushed, making actuation redundancy a necessary condition for a cable-driven system. Therefore, to apply controlled external joint torque at the hip and knee joints of the two DOFs planar leg model, at least three actuated cables are required. In this work, we considered a CDLE actuated by four cables, that is, an architecture with two redundancy, to ensure feasible solution over the complete gait cycle of an individual [35].

The thigh and shank segments are represented as D_1 and D_2 with hip and knee joints as singe DOFs revolute joints, θ_1 and θ_2. Two cables are connected to each segment as shown in Fig. 1. Cables are attached on the segment at a distance r_i from the joint center and at an offset h_i from the link axis, here i represent the cable number. Cable length, l_i, is defined from the motor position, M_i, to the corresponding cable attachment point on the link.

2.1. System modeling

A leg exoskeleton is used to apply external torques at the joints, where cables are modeled as pure force at the attachment point. The dynamic model of the system can be expressed through Lagrange's approach. The equations of motion of an n-DOF system having m actuated cables is written as:

https://doi.org/10.1017/S0263574721000242 Published online by Cambridge University Press

$$\frac{d}{dt}\left(\frac{\partial L}{\partial \dot{\theta}_i}\right) - \frac{\partial L}{\partial \theta_i} = \tau_i, i = 1, 2, ..n \tag{1}$$

where L defines the Lagrangian and θ_i represent generalized joint variable. Further, τ_i represents the externally applied torque at a joint. In the absence of any other external torque, joint torques are applied by the actuated cables. Thus, $\tau_i = \tau_i{}^c$, where $\tau_i{}^c$ represents torque due to the cable forces. Using Lagrange's method, $\tau_i{}^c$ can be expressed as:

$$\tau_i{}^c = \sum_{j=1}^{m}\left(T_j \hat{l}_j . \frac{\partial r_j}{\partial \theta_i}\right) \tag{2}$$

$$\tau_i^c = \begin{bmatrix} \hat{l}_1 . \dfrac{\partial r_1}{\partial q_i} & \hat{l}_2 . \dfrac{\partial r_2}{\partial q_i} & . & . & \hat{l}_m . \dfrac{\partial r_m}{\partial q_i} \end{bmatrix} \begin{bmatrix} T_1 \\ T_2 \\ . \\ . \\ T_m \end{bmatrix} \tag{3}$$

where $m \geq n + 1$. Rearranging the above expression in the matrix form:

$$\begin{bmatrix} \tau_1^c \\ \tau_2^c \\ \vdots \\ \tau_n^c \end{bmatrix} = \begin{bmatrix} \hat{l}_1 . \dfrac{\partial r_1}{\partial q_1} & \cdots & \hat{l}_m . \dfrac{\partial r_m}{\partial q_1} \\ \vdots & \ddots & \vdots \\ \hat{l}_1 . \dfrac{\partial r_1}{\partial q_{dof}} & \cdots & \hat{l}_m . \dfrac{\partial r_m}{\partial q_{dof}} \end{bmatrix} \begin{bmatrix} T_1 \\ \vdots \\ T_m \end{bmatrix} \tag{4}$$

$$\tau = AT \tag{5}$$

Here, $\tau \in \mathbb{R}^{n\times 1}$ denotes the joint torque values and $T \in \mathbb{R}^{m\times 1}$ denotes the cable tension values. Further, $A \in \mathbb{R}^{n\times m}$ is referred as the structure matrix representing the linear mapping between the cable tension values and joint torques.

2.2. Tension solver

As $m \geq n + 1$, Eq. (5) represents an underdetermined system. For a full ranked A, the solution of Eq. (5) can be computed from the particular solution and homogeneous solution components using the Moore Pseudo inverse, A^*, and null space, $\eta(A)$, of A respectively [36]:

$$T = A^*\tau + \eta(A)\lambda \tag{6}$$

$$\eta(A) = \{z \in \mathbb{R}^{m\times(m-n)} | Az = 0\}$$

Here, λ denotes an arbitrary scalar. Thus, for cases of nonempty $\eta(A)$, the system can have multiple valid cable tension distributions to generate the desired joint torque. For the considered general CDLE architecture, $\tau \in \mathbb{R}^{2\times 1}$, $T \in \mathbb{R}^{4\times 1}$, and $A \in \mathbb{R}^{2\times 4}$. Noting the positive cable tension constraint, $T \geq 0$, Eq. (6) generates a convex set of feasible cable tension values. Thus, an optimization problem can be formulated to find an optimal cable tension distribution. In literature [37, 38], numerical optimization methods have been successfully implemented. In this work, a quadratic programming problem is formulated to solve for cable tension distribution along the full gait cycle and is given by:

$$\min: f(\mathbf{t}) = \frac{1}{2}(T - T_P)^T(T - T_P) \tag{7}$$

$$s.t: AT = \tau \quad \text{and} \quad T_{\min} \leq T \leq T_{\max} \tag{8}$$

Here, column vector T_P is a constant vector to allow only nonzero positive cable tensions. Further, $T_{\min}$ and $T_{\max}$ denote the lower and upper limits on the cable tension values.

https://doi.org/10.1017/S0263574721000242 Published online by Cambridge University Press

2.3. Stiffness modeling

For a serial-chain manipulator, external torques are applied at the joints to allow the joint motion. Thus, for a quasi-static condition, a small variation in the joints motion can be related to the joint torques by the joints stiffness:

$$\begin{bmatrix} d\tau_{hip} \\ d\tau_{knee} \end{bmatrix} = \begin{bmatrix} K_{HH} & K_{HK} \\ K_{KH} & K_{KK} \end{bmatrix} \begin{bmatrix} d\theta_{hip} \\ d\theta_{knee} \end{bmatrix} \tag{9}$$

$$d\tau = \mathbf{K} d\theta \tag{10}$$

where $\mathbf{K}$ is defined as multi-joint stiffness matrix which denotes the relation between joint torques and angles. Elements K_{HH} and K_{HK} represent stiffness at hip joint and elements K_{KH} and K_{KK} represent stiffness at knee joint. From the relation between τ and A in Eq. (5), we get

$$d\tau = (dA)T + A(dT) \tag{11}$$

$$\text{such that, } \mathbf{K} d\theta = (dA)T + A(dT) \tag{12}$$

dT in Eq. (12) is a vector denoting small change in cable tension values which can be related to change in cable lengths through cable stiffness, k_c:

$$dT = k_c dl \tag{13}$$

Here, dl is a vector denoting change in cables lengths. Further, the rate of change of cable length can be related to joint rates as:

$$dl = -A^T (d\theta) \tag{14}$$

Substituting Eqs. (13) and (14) in Eq. (12) results in:

$$\mathbf{K} d\theta = (dA)T - A k_c A^T d\theta \tag{15}$$

Here, k_c is cable stiffness matrix. The cables are assumed to have linear stiffness property making k_c a diagonal matrix with cable stiffness constant of each cable as the diagonal element. Further, dA can be written as:

$$dA = \sum_{i=1}^{n} \frac{\partial A}{\partial \theta_i} d\theta_i \tag{16}$$

Thus, we have

$$\mathbf{K} = \underbrace{\left[\frac{dA}{d\theta_1} T \quad \frac{dA}{d\theta_2} T \quad \cdots \quad \frac{dA}{d\theta_n} T \right]}_{K_d} - \underbrace{A k_c A^T}_{K_c}$$

$$\begin{bmatrix} K_{HH} & K_{HK} \\ K_{KH} & K_{KK} \end{bmatrix} = \begin{bmatrix} K_{d_{HH}} & K_{d_{HK}} \\ K_{d_{KH}} & K_{d_{KK}} \end{bmatrix} - \begin{bmatrix} K_{c_{HH}} & K_{c_{HK}} \\ K_{c_{KH}} & K_{c_{KK}} \end{bmatrix}$$

$$\mathbf{K} = \mathbf{K}_d + \mathbf{K}_c \tag{17}$$

From the expressions of term $\mathbf{K}_d$ and $\mathbf{K}_c$, it is evident that the overall multi-joint stiffness matrix, $\mathbf{K}$, of the cable-driven system is a function of: (i) cable tension distribution, (ii) stiffness of each cable, and (iii) the structure matrix, that is, architecture of the system, which means motor positions and cable attachment points on the links.

3. Human–CDLE interaction

During walking, the lower limb movements are coordinated to move the body forward. In particular, a sequence of single foot support and double feet support phases are executed by the two limbs as

https://doi.org/10.1017/S0263574721000242 Published online by Cambridge University Press

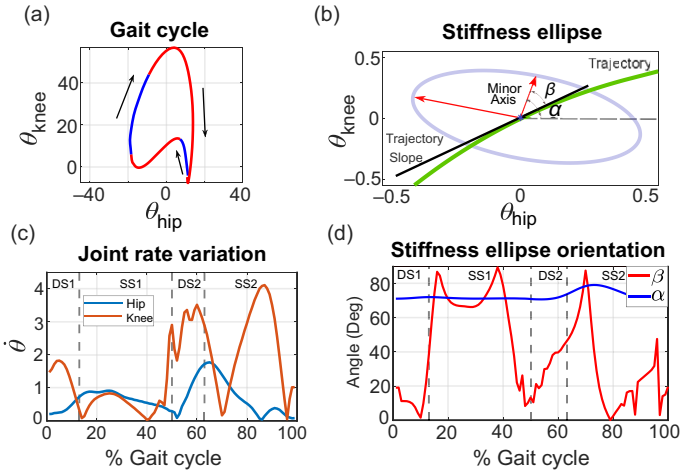

Figure 2. *(a) Hip and knee joints variation in the sagittal plane of walking [34]. (b) Stiffness ellipse at a point on the ($\theta_{hip} - \theta_{knee}$) trajectory, highlighting the ellipse's axes, and orientation angles, α and β. (c) Hip and knee joints rate variation over the gait cycle. Hip joint motion is dominant during the SS1 phase, and knee joint motion dominates the rest of the gait cycle. (d) Variation of stiffness ellipse's orientation angles, α and β, over the gait cycle for general CDLE architecture.*

are shown in Fig. 2. A gait cycle, defined from a heel strike to the following heel strike of the same limb, comprises of two single support phases (SS1 and SS2) and two double support phases (DS1 and DS2). Notably, the phases during which a single foot remains in contact with the ground and in the air are referred as stance and swing phases, respectively. Figure 2(a) shows a typical healthy individual's variation of knee and hip joint over a full gait cycle [34]. Figure 2(c) presents the rate of change of hip and knee joints along the gait cycle. One full gait cycle is divided into 100 intervals where important gait phases are defined as double support phases (DS1:1–13% of gait cycle; DS2:50–63% of gait cycle), and single support phases (SS1: 13–50% of gait cycle; SS2:63–100% of gait cycle). It is noted from Fig. 2(c) that the variations in the knee joint angle are larger during the double support phases, DS1 and DS2, as well as during SS2. Comparatively, hip joint motion is dominant during SS1.

A typical approach in using a leg exoskeleton during a gait rehabilitation training is to assist the sagittal plane motion of the disabled leg. This is achieved through the application of external torque at the hip and knee joints. Multi-joint stiffness is used as a measure to model the human–robot interaction in this work. In particular, stiffness ellipse [39] are formulated for the stiffness matrix, **K**, over the gait cycle. Figure 2(b) highlights the stiffness ellipse plotted at some point of the ($\theta_{hip} - \theta_{knee}$) trajectory in the joint space. The length of major and minor axes and the orientation of the stiffness ellipse are governed by the eigen values and corresponding eigen vectors of the stiffness matrix, **K**, respectively. Such that the stiffness ellipse at a point of ($\theta_{hip} - \theta_{knee}$) trajectory represents the direction and magnitude of the resisting joint torque to a unit change in the joint angle values. Essentially, the major axis represents the maximum resistance to the joint angle variations along that direction, and the minor axis represents the direction of least resistance. Further, the ratio of the highest to lowest eigen values, condition number[40], is a measure that reflects the isotropic nature of the stiffness matrix. This ratio that is equal to unity implies equal resistance to the joint motion variations along both the axes, that is, the isotropic stiffness case.

Thus, for the case of a CDLE applying external joint torque at the leg joints, the stiffness ellipse reflects the imposed resistance on the human leg. During a robotic gait rehabilitation paradigm, such representation can provide an understanding of the human–robot interaction. In particular, the orientation of the minor and major axes with the desired joint motion provides the orientation of the imposed resistance by the CDLE to execute that trajectory. Angle β, shown in Fig. 2(b), is defined to record the orientation of minor axis with the slope of ($\theta_{hip} - \theta_{knee}$) trajectory. Wherein, small value of angle β

https://doi.org/10.1017/S0263574721000242 Published online by Cambridge University Press

Table I. *Motor positions (in m) of general CDLE with respect to reference frame, **O** shown in Fig. 1.*

Model	M_1	M_2	M_3	M_4
General CDLE	[0.5, 0]	[1, 0]	[− 1, 0]	[− 0.5, 0]

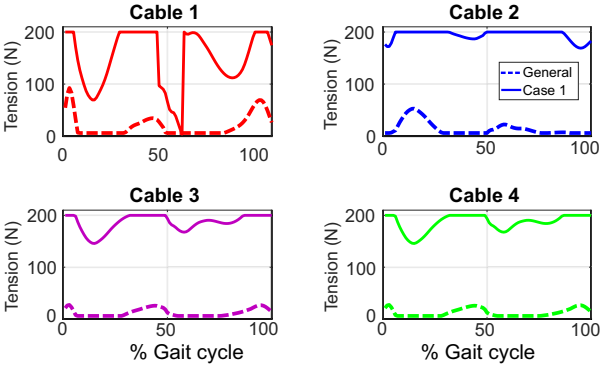

Figure 3. *Cable tension distribution for the general CDLE architecture over the complete gait cycle. Notably, large values of cable tensions are reported for the Case 1, where the cable tension distribution is optimized to minimize the stiffness matrix component K_{HH}.*

(minimum 0) represents a case where the CDLE impose minimum resistance to the desired variations in the joint motion. In contrast, a large value of β (maximum 90) implies a large resistance to the desired variations in the joint motion, which naturally signify undesirable human–robot interaction as it may lead to undesirable adaptation. Moreover, angle α is defined to measure the orientation of the imposed resistance with the joint angles. Such that a small value of α (minimum 0) represents the case of less resistance to the desired hip joint motion, while a large value (maximum 90) represents large resistance to the desired hip joint variations.

3.1. Stiffness analysis

In this work, for the human–CDLE system, it is considered that the CDLE applies torque at the hip and knee joints equivalent to 30% of the corresponding anatomical joint torque requirements. Thus, Eq. (5) is solved for the required cable tension values during a gait cycle with 0.1 and 100 N as the $T_{\min}$ and $T_{\max}$ values, respectively, for the system parameters listed in Table I. Figure 3 presents the tension distribution during the gait cycle. Equation (17) is used to compute the stiffness matrix, **K**, considering the cable stiffness values of 2.5 N/mm for the four cables. The distribution of the elements of stiffness matrix, **K**, along the gait cycle is plotted in Fig. 4.

Stiffness ellipse orientation angles, α and β, cable tension distribution, and the stiffness matrix, **K**, components are plotted in Figs. 2(d), 3, and 4, respectively, for the general CDLE architecture. The values of angle α remain large throughout the gait cycle, which imply that to apply the desired joint torque assistance during the gait cycle, the general CDLE architecture induced a large resistance at the hip joint. Noting the variations of the stiffness matrix component, K_{HH}, which accounts for the stiffness at the hip joint due to the hip joint motion, it is observed that component K_{HH} values are much larger than any other component of the stiffness matrix, **K**, throughout the gait cycle as shown in Fig. 4. From Fig. 2(d), the angle β demonstrates many changes in its values, reaching a maximum of 90 and a minimum of 0 *deg* over the gait cycle. This implies that to apply the desired joint torque assistance, the CDLE induces joint stiffness with minor axis not always along the desired variations in the hip and knee joint angles. In particular, the angle β is smaller during DS1, transition between SS1 and DS2, and late

https://doi.org/10.1017/S0263574721000242 Published online by Cambridge University Press

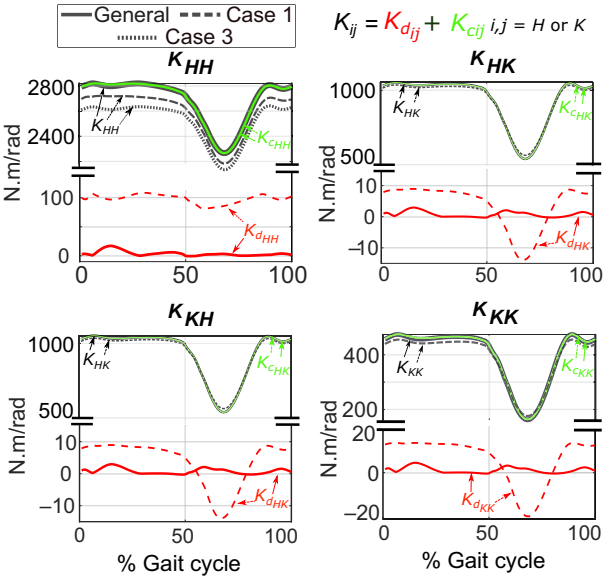

Figure 4. *The components of the stiffness matrix,* ***K****, over the gait cycle for the general CDLE architecture, and stiffness modulation Case 1 and 3. The contribution of K_d and K_c terms is highlighted for the stiffness matrix components. It is observed that the values of K_c dominates over the gait cycle compared to K_d. Modulation of* ***K*** *using cable tension resulted in increase in the K_d but not very significant compared with K_c values.*

SS2 phases. Noting from Fig. 2(c) and (d), it is observed that these phases correspond to leg movements that require higher knee joint range of motion. In contrast, the angle β has large values mostly during SS1, transition between DS2 and SS2, and early SS2 phases, during these phases the required hip joint range of motion is higher than the knee joint.

The variations in the α and β values, and the large values of stiffness matrix component, K_{HH}, imply that the general CDLE architecture poses a higher stiffness at the hip joint throughout the gait cycle, such that it resists the desired changes in the hip joint motion more than the knee joint motion. As the act of walking requires sufficient contribution of both joints, the applied human–CDLE interaction in this case may result in a preference toward distal joint strategy. In general, during a robotic rehabilitation training paradigm, external forces are applied to assist the joint movement, but the human–robot interaction is typically not modeled and optimized for. In the case of CDLE, the flexibility in changing the cable routing and attachment points, and the existence of multiple cable tension solution provides the advantage of assisting the required joint motion along with the possibility of establishing a desired human–robot interaction. The following sections of this paper present the stiffness matrix, **K**, modulation through different system characteristics of a CDLE to achieve a desired human–CDLE interaction, that is, lower value of angle β over a gait cycle.

3.2. Stiffness modulation

From Eq. (17), it is observed that the stiffness matrix, **K**, depends on the cable elasticity, motor positions, cable attachment positions, and cable tension distributions. Variation in these parameters can result in desirable tuning of the human–CDLE interaction, modeled as the imposed stiffness at the joints. In particular, the effect of the cable tension distribution, motor positions, cable stiffness, and cable routing on the stiffness matrix, K, are studied. The stiffness analysis of the general CDLE architecture in the previous section noted a higher stiffness at the hip joint, thus, one approach to improve the human–robot interaction is to optimize a system parameter to reduce the stiffness matrix component, K_{HH}.

https://doi.org/10.1017/S0263574721000242 Published online by Cambridge University Press

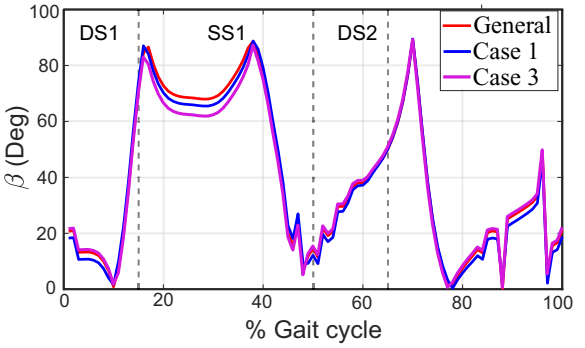

Figure 5. *Variation of the stiffness ellipse's orientation angle, β, for the general CDLE architecture and for stiffness modulation Case 1 and Case 3. Notably, no significant change is observed in angle β values for Case 1 and Case 3.*

Case 1: Cable tension distribution

An optimization problem is formulated to minimize K_{HH}, that is, the component of the stiffness matrix that represents the resistance at the hip joint due to the small variations in the hip joint motion. This problem is solved for an alternate cable tension distribution during the gait cycle while still generating the required 30% anatomical joint torque assistance at the hip and knee joints. An alternate cable tension distribution will alter the component K_d in Eq. (17), which will modify the overall stiffness matrix, **K**:

$$\min : K_{HH} = f(T_1, T_2, T_3, T_4) \tag{18}$$

$$s.t : AT = \tau, T_{\min} \leq T \leq T_{\max}$$

Cable tension limits $T_{\max}$ and $T_{\min}$ are retained as 200 and 0.1 N, respectively, and cable stiffness values are taken as 2.5 N/mm.

The cable tension distribution that minimizes K_{HH} is shown in Fig. 3. It is observed that the cable tension values increased among all the cables. From Fig. 4, it is observed that the new cable tension distribution results in the reduction of the K_{HH} values over the gait cycle but not the other components of the stiffness matrix, that is, K_{KK} and K_{KH} or K_{HK}. Furthermore, resolving each of the **K** components into the corresponding K_d and K_c components as per the definitions in Eq. (17), significant changes are observed only in the K_d values, but the K_c values remained almost same between the general CDLE and Case 1 conditions. One vital observation from Fig. 4 is about the large magnitude difference of the K_c values from the K_d values, which meant only a small reduction in the K_{HH} values. The component K_c majorly factors in the contribution of the system geometry and cable elasticity, the results essentially imply the dominance of these factors over the cable tension distribution, and similar observations were reported for cable-driven parallel architectures [41]. One way to allow even greater changes in K_d can be to permit higher cable tension limits, but for the human application the CDLE applying large cable tension would only result in undesirable human–CDLE interaction. Notably, for the Case 1, no significant changes are reported in the orientation angle β values compared to the general CDLE β values over the gait cycle, as shown in Fig. 5. Thus, the variations in the cable tension distribution alone may not be able to tune the the human–CDLE interaction during a rehabilitation paradigm.

Case 2: Motor positions

As noted from the large K_c values in the Case 1, the dominant role of system geometry toward the overall stiffness matrix, **K**. In this section, to modulate the stiffness matrix, **K**, the system geometry is altered. In particular, the motor positions are optimized, which can also be thought of as optimizing the cable anchoring at the frame to obtain a desirable human–CDLE interaction. Thus, an

https://doi.org/10.1017/S0263574721000242 Published online by Cambridge University Press

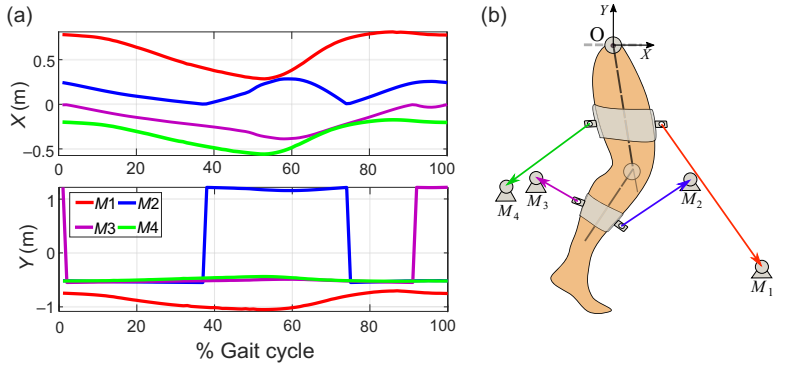

Figure 6. *(a) Case 2: Optimum motor positions along the gait cycle to minimize the hip stiffness $K_{c_{HH}}$ for the general CDLE. (b) General CDLE configuration at 15% of gait cycle based on the motor positions in part (a), $M_1 = [0.7, -0.86]$, $M_2 = [0.12, -0.53]$, $M_3 = [-0.11, -0.53]$, $M_4 = [-0.27, -0.54]$, that facilitates the lower $K_{c_{HH}}$ values.*

objective function is formulated to minimize the $K_{c_{HH}}$ element of K_c by solving for the optimal motor positions. Lower values of $K_{c_{HH}}$ will reduce the K_{HH} component of the stiffness matrix, **K**. Let $M = [M_{1x}, M_{1y}, M_{2x}, M_{2y}, M_{3x}, M3_{3y}, M_{4x}, M_{4y}]$ be the vector of motor positions with respect to origin, O, as shown in Fig. 1:

$$\min : K_{c_{HH}} = f(M) \tag{19}$$

$$s.t : M_{ix} \in [0.1, 2],\ i = 1, 2\ \ M_{ix} \in [-2 - 0.1],\ i = 3, 4$$
$$M_{iy} \in [-1, 1],\ i = 1, ..4$$

The choice of bounds on the motor positions are as per the coordinate system indicated in Fig. 1 and to facilitate hip and knee joints actuation in the sagittal plane of walking. The results of the optimization are plotted in Fig. 6, highlighting the four motor positions and a CDLE configuration at 15% of the gait cycle.

To minimize $K_{c_{HH}}$, the optimization process led to the changes in all four motor positions differently over the gait cycle. It is observed that for most part of the gait cycle, all four motors need to be below the hip joint, indicated by negative y-values. In particular, y-component for M_1 and M_4 are always negative. In contrast, y-position of M_2 and M_3 shown significant jump. Thus, to achieve lower values for $K_{c_{HH}}$, motors M_1 and M_4 must be below the hip joint. Further, the changes in x-values for the four motors reflect that cables connected to thigh segment should be anchored away from the leg segment and cables connected to the shank should be anchored close to the leg segment.

Solving for the cable tension values using Eq. (7) for these new motor positions, say at 15% of the gait cycle as shown in Fig. 6(b), did not give a feasible tension distribution. This is because motors below the hip joint cannot apply 30% hip joint torque with positive cable tension. Thus, the optimized motor positions are not suitable for the required joint torque assistance. Notably, the changes in the y-direction of the motor position are relevant to reduce $K_{c_{HH}}$ component, which has been noted to dominate. Thus, the prospects of reducing K_{HH} component to improve the human–CDLE interaction is to reduce $K_{c_{HH}}$ element by bringing the motors, or cable anchoring, below the hip joint. However, the CDLE architecture has to be modified appropriately to achieve the feasible cable tension distribution.

Case 3: Effect of cable stiffness

Variations of other parameters, such as distance of cable attachment from joints, r_i, and the offset cable attachment on the leg segment, h_i, can also alter the CDLE geometry but noting the limited amount of changes that can be accommodated in these parameters, the reduction in the already very large values

https://doi.org/10.1017/S0263574721000242 Published online by Cambridge University Press

of hip stiffness terms K_{HH} and K_{HK} cannot be significant. Notably, one parameter whose value can be varied to alter the K_c term of the K_{HH} component is the cable stiffness, that is, parameter k_c as defined in Eq. (13). From the expression of K_c in Eq. (17), a different value of k_c results in different K_c even when CDLE geometry and required cable tension distribution remain same. To highlight this aspect, the results, when the value of k_c is changed from 2.5 to 1.5 N/mm, for only cables 1 and 4 are presented in Figs. 4 and 5. Noting the expression of K_c in Eq. (17), changes in cable stiffness of cables 1 and 4 affect only the K_{HH} component of the stiffness matrix. Small reduction in the values of K_{HH} can be observed in Fig. 4, but these changes are not enough to show significant changes in the human–CDLE interaction as noted by insignificant change in the angle β values for Case 3 in Fig. 5. Reducing k_c values further may show further reduction in the K_{HH} term, but a cable with low stiffness might not be practically suitable for applying controlled external forces to assist the joint torque. However, without adequate modification in the architecture, the dominant role of K_{HH} cannot be compensated by such system parameter alterations. Thus, the following section considers the possibility of altering the cable routing to provide a CDLE architecture that achieves the required condition to alter the human–CDLE interaction goal.

4. Co-shared CDLE architecture

Considering the formulation of the structure matrix, **A**, for the general CDLE in Eqs. (4) and (5), it is observed that the torque at the proximal hip joint has components from the cables attached to thigh as well as shank segments. Thus, the serial-chain architecture of the CDLE itself leads to high stiffness component at the hip joint to the hip joint motion, K_{HH}. The optimization problem, Case 2, in the last section proposes to alter the cable routing, so as to reduce the effect of distal knee joint actuation on the hip joint stiffness.

Noting the effect of cable anchoring at the frame and constraint of positive cable tension distribution, a co-shared CDLE architecture as shown in Fig. 7 is considered. In this case, cables 2 and 3 routing from the shank segment to the frame, or motors, through the thigh segment provide a means to knee actuation as well as hip actuation. With this new architecture, the effect of knee joint actuation on hip joint stiffness is reduced. Taking the example of cable 2 in the two architectures, general CDLE as in Fig. 1 and co-shared CDLE as in Fig. 7, a positive T_2 value will result in positive external torque at both the knee and hip joints in the general CDLE case; however, the same cable tension value will apply a positive torque at knee and either negative or positive torque at hip joint in the co-shared CDLE, as cable 2 has dynamic anchor points at the thigh segment which are a function of the leg motion.

4.1. Structure matrix formulation

Co-sharing of the cables in the CDLE modifies the mapping between the cable tension distribution and the joint torque values, that is, the structure matrix, **A**. In particular, the expressions for cables 1 and 4 in Eqs. (4) and (5) remain the same, but for the co-shared cables 2 and 3 they get modified. With the assumption of no friction at the thigh connection, the cable tension value in the co-shared cables does not change. The contribution of cable 2 tension, T_2, on the hip and knee joints torques, τ_1^c and τ_2^c , is shown in Fig. 7 and given as follows [42]:

$$\begin{bmatrix} \tau_1^c \\ \tau_2^c \end{bmatrix} = \begin{bmatrix} \hat{l}_{22}\dfrac{\partial \vec{r}_2}{\partial \theta_1} + (\hat{l}_{21} - \hat{l}_{22})\dfrac{\partial \vec{r}_1}{\partial \theta_1} \\ \hat{l}_{22}\dfrac{\partial \vec{r}_2}{\partial \theta_2} \end{bmatrix} [T_2] \tag{20}$$

Here, $\hat{l}_{22}$ and $\hat{l}_{21}$ are vectors from the cable attachment point on the shank to the thigh segment and from thigh to motor position M_2, respectively. Further, the first torque term in τ_1^c is due to the shared part of cable 2 between the shank and thigh, while the second torque term is due to the cable 2 routed from the

https://doi.org/10.1017/S0263574721000242 Published online by Cambridge University Press

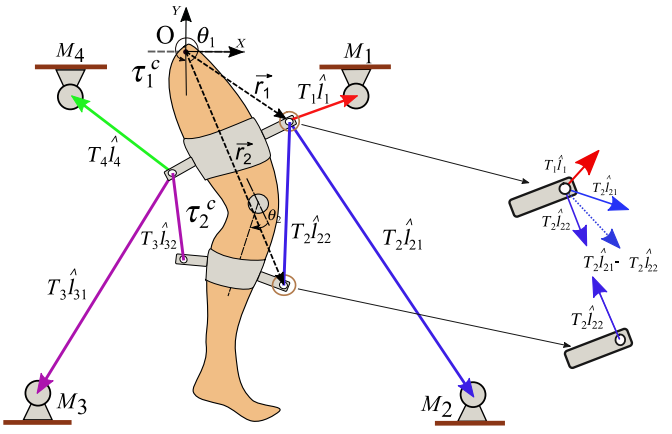

Figure 7. *Co-shared CDLE architecture: distal joint cables 2 and 3 attached to shank segment, routed through the thigh attachment points to their motor actuation position. Essentially cable routing point on thigh segment serves as dynamic anchor point for a cable originating at the distal segment. Link lengths, D_i, cable attachment points, r_i, and offset position, h_i, are retained similar as for the general CDLE architecture.*

thigh segment to the anchor point at the frame, motor position M_2. Similar expression will be there for cable 3, such that the modified structure matrix, **A**, is given as:

$$\begin{bmatrix} \tau_1^c \\ \tau_2^c \end{bmatrix} = \begin{bmatrix} \hat{l}_1 \dfrac{\partial \vec{r}_1}{\partial \theta_1} & \hat{l}_{22} \dfrac{\partial \vec{r}_2}{\partial \theta_1} + (\hat{l}_{21} - \hat{l}_{22}) \dfrac{\partial \vec{r}_1}{\partial \theta_1} & \hat{l}_{32} \dfrac{\partial \vec{r}_3}{\partial \theta_1} + (\hat{l}_{31} - \hat{l}_{32}) \dfrac{\partial \vec{r}_4}{\partial \theta_1} & \hat{l}_4 \dfrac{\partial \vec{r}_4}{\partial \theta_1} \\ \hat{l}_1 . \dfrac{\partial \vec{r}_1}{\partial \theta_2} & \hat{l}_{22} \dfrac{\partial \vec{r}_2}{\partial \theta_2} & \hat{l}_{32} \dfrac{\partial \vec{r}_3}{\partial \theta_2} & \hat{l}_4 . \dfrac{\partial \vec{r}_4}{\partial \theta_2} \end{bmatrix} \begin{bmatrix} T_1 \\ T_2 \\ T_3 \\ T_4 \end{bmatrix} \tag{21}$$

4.2. Human–CDLE interaction: Co-shared case

The co-sharing of cables provides the flexibility in shifting the anchor points, motor positions, below the hip joint for cables actuating the hip joint to incorporate the required condition of positive cable tension distribution. Thus, co-shared CDLE architecture can impose lower stiffness component $K_{c_{HH}}$ to improve the human–CDLE interaction, if the motors 2 and 3 positions are optimized:

$$\min : K_{c_{HH}} = f(M) \tag{22}$$

$$s.t : M_{2x} \in [0.1, 2],\ M_{3x} \in [-2, -0.1]$$
$$M_{iy} \in [-1, 2], i = 2, 3$$

Lower and upper bounds for the above optimization problem are similar to that of general CDLE Case 2, Eq. (19). The optimized motor positions are plotted in Fig. 8. The y-positions of the two motors remain close to the lower bound over the gait cycle with some fluctuations in M_3 for part of the gait cycle. Further, the x position of the two motors indicate cable anchoring away from the leg segment at the start and end of the gait cycle and close to the leg segment anchoring around 50% of the gait cycle. From these variations, motor positions as indicated in Table II are finalized for further analysis, where mean values over the gait cycle for M_2 and M_3 are taken, and sudden fluctuations in M_3 are not considered.

Solving Eq. (8) for the co-shared CDLE parameters, the cable tension distribution to assist 30% of the anatomical joint torque requirement at the hip and knee joints over the gait cycle is shown in Fig. 9. Compared to the general CDLE architecture, for the co-shared CDLE, lower tension values for

https://doi.org/10.1017/S0263574721000242 Published online by Cambridge University Press

Table II. *Motor positions (in m) of co-shared CDLE with respect to reference frame, **O**, as shown in Fig. 7.*

Model	M_1	M_2	M_3	M_4
Co-Shared	[0.3, 0]	[0.45, −0.84]	[− 0.47, −0.9]	[− 0.3, 0]

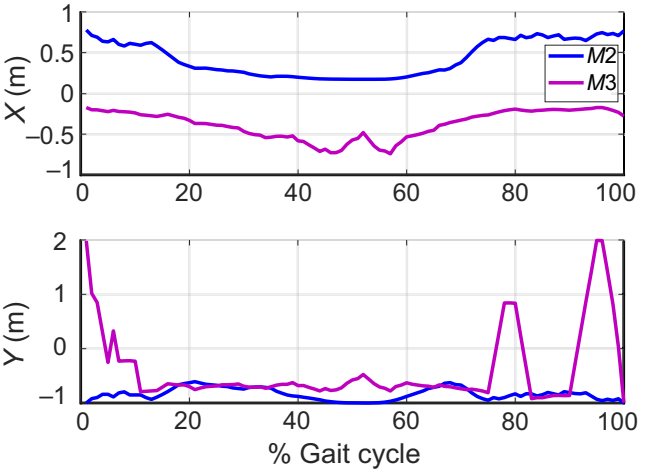

Figure 8. *Motor positions, M_2 and M_3, for the co-shared architecture over the gait cycle that facilitates reduction in the hip joint stiffness term, K_{cHH}.*

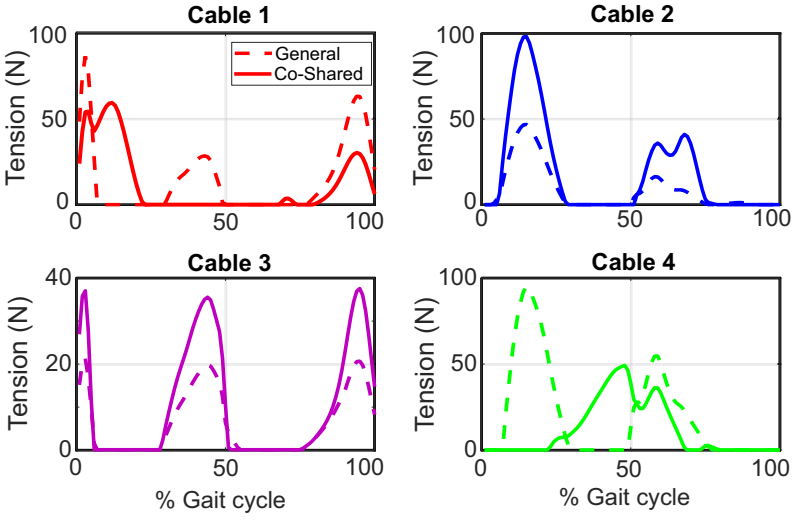

Figure 9. *Cable tension distribution for the general CDLE and co-shared CDLE architectures. Cable co-sharing resulted in increase in the tension values for cables 2 and 3, and lower tension values for cables 1 and 4.*

cables 1 and 4 and higher tension values for co-shared cables 2 and 3 are required to apply the desired joint torques. Due to the co-sharing, higher tension force is required in cables 2 and 3 to account the dynamic anchoring and reduced moment arm for the knee joint. Further, the tension forces in cables 2 and 3 also contribute in the required hip joint torque over the gait cycle. The stiffness matrix components

https://doi.org/10.1017/S0263574721000242 Published online by Cambridge University Press

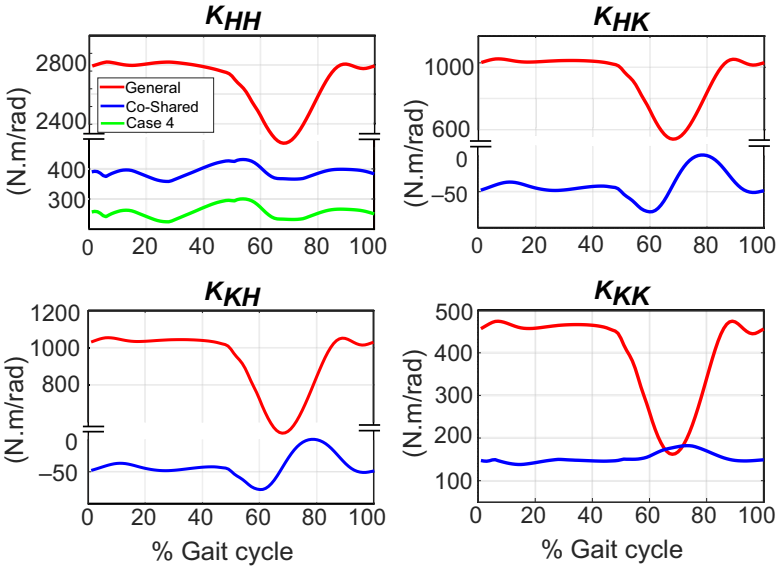

Figure 10. *Variations of the stiffness matrix components values over the gait cycle for the general CDLE, co-shared CDLE, and Case 4. Co-sharing of cables resulted in reduction in the magnitude of imposed stiffness by the CDLE. These values are further reduced for Case 4.*

for the co-shared CDLE architecture over the gait cycle are plotted in Fig. 10. A significant reduction is observed in all the stiffness components of the stiffness matrix, **K**, for the co-shared CDLE compared to the general CDLE. Due to the co-sharing, the torque resistance at the hip joint to the hip joint motion, K_{HH}, reduced by around 86% of its value for most of the gait cycle for the general CDLE case. Similarly, the reduction in K_{KK} component is around 66%.

The overall effect of the changes in the stiffness matrix components and stiffness ellipse orientation angle, β, variation over the gait cycle are highlighted in Figs. 11 and 12. A striking distinction is observed among the general CDLE and co-shared CDLE architectures. For the co-shared CDLE in comparison with the general CDLE case, the orientation of the stiffness ellipse as well as its size changed, such that the CDLE applies required external joint torques while favoring the desired hip and knee joints motion during the gait cycle. In particular, Fig. 12 highlights that the minor axis of the stiffness ellipse is better aligned with the $(\theta_{hip} - \theta_{knee})$ trajectory, that is, lower angle β values. Further, Fig. 11 notes the reduction in the condition number to imply reduced stiffness ellipse size and its isotropic nature.

Case 4: Effect of cable stiffness

The effect of cable tension distribution, geometry, and cable routing on the stiffness matrix has been presented in the above analysis to explicate the stiffness performance of a CDLE. These system parameters can further be tuned to further optimize the performance, but one parameter whose value can also be varied is the cable stiffness, k_c. As noted in Case 3 of general CDLE architecture, a different value of k_c for cables 1 and 4 only reduces the K_c term of K_{HH}. Unlike the results for Case 3 with general CDLE architecture, the change in the value of k_c from 2.5 to 1.5 N/mm for cables 1 and 4 demonstrates a significant improvement of human–CDLE interaction for the co-shared architecture. These results are highlighted in Figs. 10, 11, and 12. The observed results indicate further improvement in the human–CDLE interaction, such that the imposed multi-joint resistance to the desired joint motion by the CDLE reduces.

https://doi.org/10.1017/S0263574721000242 Published online by Cambridge University Press

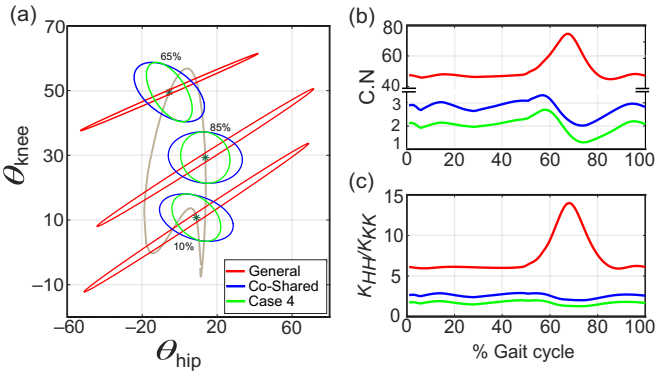

Figure 11. *(a) Stiffness ellipse plotted at 10, 65, and 85% of the gait cycle to highlight the effect of the changes in imposed multi-joint stiffness between general CDLE, co-shared CDLE, and Case 4. (b) Condition number variation for these three cases. Large values for the general CDLE case imply anisotropic nature of the imposed stiffness. (c) Ratio of stiffness matrix components, K_{HH} and K_{KK}, over the gait cycle for the three cases. Hip stiffness dominance over knee stiffness term reduced for co-shared CDLE.*

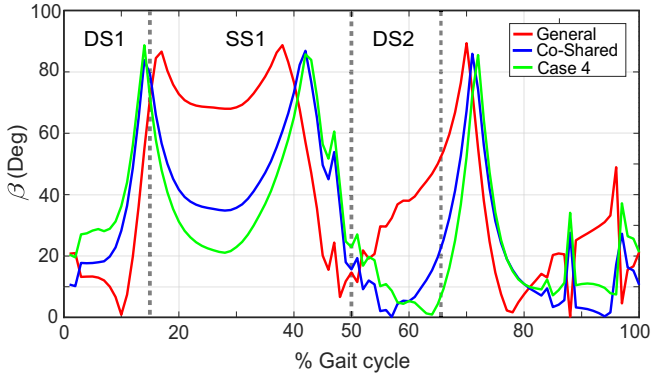

Figure 12. *Stiffness ellipse's orientation angle, β, variations over the gait cycle for the general CDLE, co-shared CDLE, and Case 4. Smaller values of β were reported for the co-shared architecture, which imply reduction in imposed resistance along the desired joint motion and highlight improved human–CDLE interaction during the gait assistance.*

Inferences

The stiffness ellipse plots in Fig. 11(a) for the general and co-shared CDLE architectures at 10, 65, and 85% of the gait cycle highlight the changes in the multi-joint stiffness between the two architectures. Firstly, the stiffness ellipses drawn for the general CDLE are highly skewed, which is also reflected by the large ratio of eigen values, that is, large condition number. This reflects the anisotropic nature of imposed resistance by the CDLE, that is very large resistance to joint variations along the major axis and a very small resistance to joint motion along the minor axis while applying for the required joint assistance. Notably, for the general CDLE at 10% of the gait cycle, where β value is low in Fig. 12, there is less resistance to the desired joint motion, but at other points of the gait cycle where corresponding β values are large, the general CDLE imposes large resistance which may lead to undesirable leg joint movements. In contrast, the stiffness ellipses for the co-shared CDLE are close to being symmetrical, implied by the low condition number values over the gait cycle. This essentially means that CDLE with

https://doi.org/10.1017/S0263574721000242 Published online by Cambridge University Press

co-shared cables imposes comparable resistances to the joint motion along the major and minor axes. Thus, the possibilities of undesirable joint motion adaptation are lower in the case of co-shared CDLE.

Both the general and co-shared CDLE architectures impose a large stiffness at the hip joint compared to the knee joint. However, the ratio K_{HH}/K_{KK} plotted in Fig. 11(c) is large and exhibits a significant increase in its value during the gait cycle for the general CDLE. For the co-shared CDLE, this ratio is smaller and remains mostly constant over the gait cycle. Noting the variations in the stiffness components in Fig. 10, the large ratio of K_{HH}/K_{KK} implies a large value of imposed resistance at the hip to the hip joint motion compared to imposed resistance at the knee joint to knee joint motion. Furthermore, the increase in this ratio reflects a relative increase in the imposed resistance at the hip joint to the hip joint motion for that part of the gait cycle. Thus, in the case of general CDLE, the imposed human–CDLE interaction may lead to a preference toward the distal joint strategy resulting in undesirable adaptation in the hip and knee joints motion during walking. In contrast, the imposed human–CDLE interaction for the co-shared CDLE imposes comparable stiffness levels at the hip and knee joints and steadily alters these levels over the gait cycle to apply the desired joint torques. Thus, the co-shared architecture with such stiffness characteristics is less likely to create distal versus proximal joint preference during a CDLE-based gait rehabilitation paradigm.

The current work models the human–robot interaction through the multi-joint stiffness formulation of the redundantly actuated CDLE. The stiffness performance of a CDLE architecture while applying the assistance of 30% at the hip and knee joints is evaluated as the imposed resistance at the joints. The orientation of the direction of less resistance, the minor axis of the stiffness ellipse, with the desired hip and knee joints trajectory, and angle β, is presented for different cases. Overall, it is observed that the changes in the CDLE parameters with general architecture did not affect the stiffness performance significantly. Notably, change in the cable routing to have two co-shared cables between the thigh and shank segments resulted in significant changes in the stiffness measures. Even though the minor axis of the stiffness ellipse is not along the desired hip and knee joints trajectory's slope, from Fig. 12, the angle β values for co-shared CDLE are significantly less than the corresponding values of general CDLE for the most part of the gait cycle. These reduced β values reflect a reduction in the imposed resistance by the CDLE at the joints, which essentially imply an improvement in the human–CDLE interaction.

For a typical robotic gait rehabilitation paradigm, the major focus is on applying external forces to assist the joint motion. As a result of various studies with the existing systems [12, 13], the developmental focus in most of the recent robotic exoskeletons has been in removing the undesirable effects that the robotic system can add on the participants. In particular, the use of flexible actuation architectures is being promoted to reduce the imposed mass/inertia and remove the mobility constraints [16, 17, 24, 25]. The current work highlights the role of applied resistance at the joints by the CDLE and presents the stiffness modulation to effectively tune the human–CDLE interaction. The observed changes in the co-shared CDLE architecture case essentially reflect the inherent coupling and adaptation among the human lower limb joints. Noting the desired limb movement during walking, a significant contribution from the hip and knee joints is observed. Thus, the use of a robotic leg exoskeleton to apply external joint torques can be effective if the imposed human–robot interaction favors the desired joint motion. In particular, the case of a co-shared CDLE improved the human–robot interaction by allowing control of the imposed resistance at the hip joint. Notably, system parameters of the co-shared CDLE, such as cable stiffness, cable tension distribution, cables anchoring on the leg segments and frame, and even the cable routing, can be tuned further to facilitate required improvement in the human–CDLE interaction.

5. Multi-joint stiffness computation

In this section, experimental computation of the multi-joint stiffness, **K**, is presented for a cable-driven serial-chain manipulator. Figure 13 shows a two DOFs planar manipulator with two links representing the leg segments and corresponding joints, hip, and knee. Four cables are routed to achieve two different cable routings, that is, CDLE general and co-shared architectures in Figs. 1 and 7, respectively. During

https://doi.org/10.1017/S0263574721000242 Published online by Cambridge University Press

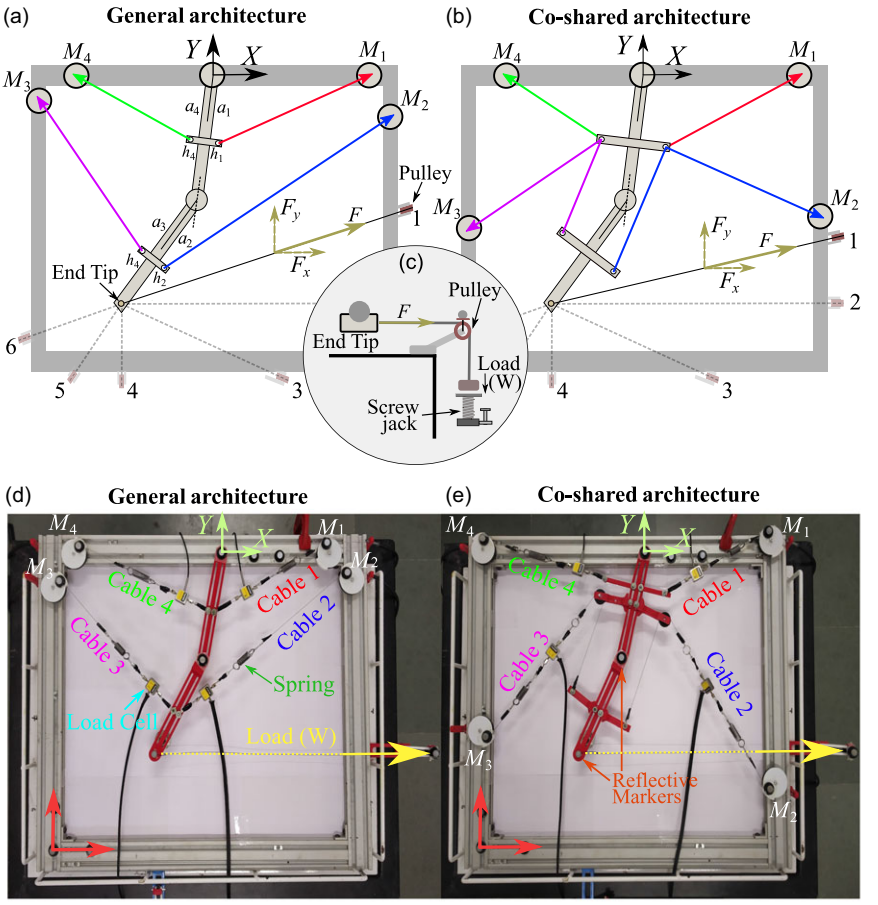

Figure 13. *(a, b) Schematic of the general and co-shared architecture setup, highlighting all six loading directions, (c) front view schematic highlighting the loading mechanism, (d) experimental setup of CDLE general architecture, and (e) co-shared architecture.*

the experiment, the manipulator is maintained at an equilibrium configuration through adequate cable tensioning. Each cable is in series with a spring, with known stiffness, and a load cell, to measure the cable tension during the experiment. For the computation of $\mathbf{K}$, a known external force vector is applied at the tip of the second link, end effector, by hanging a small dead weight using a cable and pulley arrangement as shown in Fig. 13(c).

Such application of small external force vector, F, on the manipulator in equilibrium state causes small deflection of the end effector in the taskspace, dX. Corresponding to dX, there is small deflection in the joint space, $d\theta$, that represents the effect of multi-joint stiffness, $\mathbf{K}$. Equation (23) formulates the relation between the taskspace stiffness, $\mathbf{K}_X$, and multi-joint stiffness, $\mathbf{K}$, for a manipulator incorporating the conservative congruence transformation condition [43], where manipulator Jacobian is denoted by J. For a given manipulator's configuration, θ, and external force, F, the end effector deflection, dX, is a nonlinear function of $\mathbf{K}$, refer to Eq. (24). Thus, by measuring a set of deflections, $\{dX\}$, for a set of externally applied force vector, $\{F\}$, the components of $\mathbf{K}$ are computed using a least square error estimation algorithm. Denoting dX_{th} as the theoretically computed end effector deflection values as per Eq. (23) that incorporates the unknown components of $\mathbf{K}$, and dX_e the corresponding set of experimental

https://doi.org/10.1017/S0263574721000242 Published online by Cambridge University Press

Table III. *Table provides details of the considered setup parameters for CDLE general and co-shared architectures, and corresponding theoretical and experimental values in joint space stiffness matrix are presented. Unit of spring stiffness k_{c_i} is (N/m).*

CDLE system parameters (in m)		K_{th}**(Nm/rad)**	K_e**(Nm/rad)**
General architecture		Theoretical	Experiment
$a_1 = a_4 = 0.082$ $a_2 = a_3 = 0.084$	C_1	$\begin{bmatrix} 88.44 & 26.95 \\ 26.95 & 9.71 \end{bmatrix}$	$\begin{bmatrix} 85.95 & 24.74 \\ 24.74 & 8.35 \end{bmatrix}$
$h_1 = h_2 = h_3 = h_4 = 0.005$ $M_1 = [0.175, 0.02], M_2 = [0.21, -0.02]$	C_2	$\begin{bmatrix} 80.23 & 21.13 \\ 21.13 & 6.81 \end{bmatrix}$	$\begin{bmatrix} 78.63 & 23.12 \\ 23.12 & 5.91 \end{bmatrix}$
$M_3 = [-0.35, -0.03] M_4 = [-0.24, 0.01]$ $k_{c_1} = 1231.6, k_{c_2} = 1018.25$ $k_{c_3} = 1202.75, k_{c_4} = 1157.7$	C_3	$\begin{bmatrix} 84.82 & 23.76 \\ 23.76 & 8.79 \end{bmatrix}$	$\begin{bmatrix} 88.54 & 26.28 \\ 26.28 & 9.04 \end{bmatrix}$
Co-shared architecture		Theoretical	Experiment
$a_1 = a_4 = 0.05$ $a_{21} = a_{31} = 0.073$ $a_{22} = a_{32} = 0.085$	C_1	$\begin{bmatrix} 12.36 & -0.44 \\ -0.44 & 10.97 \end{bmatrix}$	$\begin{bmatrix} 11.98 & -0.42 \\ -0.42 & 10.69 \end{bmatrix}$
$h_1 = 0.047, h_4 = 0.005$ $h_{21} = h_{31} = 0.0057$ $h_{22} = h_{32} = 0.005$	C_2	$\begin{bmatrix} 10.82 & -0.51 \\ -0.51 & 9.48 \end{bmatrix}$	$\begin{bmatrix} 11.16 & -0.57 \\ -0.57 & 9.47 \end{bmatrix}$
$M_1 = [0.201, 0.03], M_2 = [0.19, -0.31]$ $M_3 = [-0.25, -0.24] M_4 = [-0.27, -0.02]$ $k_{c_1} = 1231.6, k_{c_2} = 1018.25$ $k_{c_3} = 1202.75, k_{c_4} = 1157.7$	C_3	$\begin{bmatrix} 12.01 & -0.48 \\ -0.48 & 11.16 \end{bmatrix}$	$\begin{bmatrix} 11.58 & -0.52 \\ -0.52 & 10.33 \end{bmatrix}$

deflection values, the error is defined as $de = dX_{th} - dX_e$. Accordingly, a least square error estimation algorithm is formulated as per Eq. (25) to compute the components of $\mathbf{K}$:

$$\mathbf{K}_X = J^{-T}\left(\mathbf{K} - \underbrace{\begin{bmatrix} \frac{dJ^T}{d\theta_1}F & \frac{dJ^F}{d\theta_2}F \end{bmatrix}}_{K_g}\right)J^{-1} \tag{23}$$

$$F = \mathbf{K}_X dX \implies dX = f(\theta, \mathbf{K}, F) \tag{24}$$

$$E = \sum_j de_j{}^T de_j \tag{25}$$

The details of the experimental setup are provided in Fig. 13. To allow the horizontal planar motion of the manipulator, a small castor wheel was mounted under each link to offload the gravity term. Reflective markers were mounted on the setup to measure the link movements as well as the force application direction. A Vicon motion capture system with eight cameras was used. Further, Futek load cells were used in series with each cable to measure the real-time cable tension values. To apply the external force on the end effector, dead weights in the range of 50–200 g with 50 g increments, that is, a total of four different weights, were used. A screw jack mechanism was used to lower the dead weight to prevent its oscillations during the experiment. Six different locations, marked as 1–6 in Fig. 13, were used for mounting the pulley to generate six different force directions. For each dead weight in every direction, a total of three trials were performed. Thus, a total of $j = 72$ set of readings were recorded for a configuration of the manipulator.

The system parameters, including the cable attachment points, motor locations, and cable spring stiffness values, are listed in Table III. Figure 13(c) and (d) present the experimental setup of general

https://doi.org/10.1017/S0263574721000242 Published online by Cambridge University Press

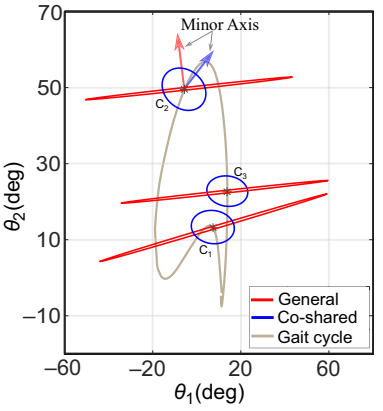

Figure 14. *Multi-joint stiffness ellipse for general and co-shared architectures plotted from the experimental data for three different configurations, C_1, C_2, and C_3. Minor axis of the ellipse that represents direction of less stiffness is shown for C_2. Co-shared architecture reported a near isotropic multi-joint stiffness behavior for all the three configurations.*

and co-shared architectures. Three different manipulator configurations, C_1, C_2, and C_3 with $[\theta_1, \theta_2] = [15°, 14°], [-5°, 49°]$ and $[17°, 22°]$, were chosen for the analysis. The experimentally computed values of multi-joint stiffness, $\mathbf{K}_e$, and the corresponding theoretical values, $\mathbf{K}_{th}$, as per Eq. (17) of the two architectures, for both the configurations are listed in Table III. For $\mathbf{K}_{th}$, the load cells data are used as the cable tension values, T, in Eq. (17). A relatively close match is observed between the theoretical and experimental components of $\mathbf{K}$. Thus, $\mathbf{K}_e$ values experimentally validates the modulation in multi-joint stiffness performance between the two CDLE architectures. Corresponding stiffness ellipses using $\mathbf{K}_e$ values are plotted in Figs. 14 to note these changes.

Essentially, for the chosen system parameters, a significant reduction in all four components of $\mathbf{K}$ is reported for the co-shared architecture compared to the general architecture, refer to Table III. In particular, the value of K_{11}, which presents the stiffness at joint 1, reduced significantly by almost 86% but remained dominant compared to K_{22}. This implies a notable reduction in the ratio of diagonal elements, K_{11}/K_{22}, and a C.N. close to unity for the co-shared architecture at different configurations. Further, the off-diagonal terms, K_{12} and K_{21}, are close to zero for co-shared architecture signifying an almost decoupled multi-joint stiffness. Accordingly, the co-shared case provides an isotropic stiffness variation compared to the general architecture case, where the direction of least resistance changes with the manipulator's configuration as represented by the minor axis orientation in Fig. 14. These observations are in accordance with the theoretical analysis presented in Section 4, refer to Figs. 11 and 12.

To bring the CDLE perspective, joints 1 and 2 of the manipulator can be represented as human hip and knee joints, respectively. Accordingly, the results imply that a general architecture compared to the co-shared architecture imposes a higher stiffness at the hip than knee joint, a coupling between the two joints, and a notable skewed resistance variations during the leg motion. Considering the anatomical joint stiffness distribution and the human ability to adapt the walking pattern in response to external physical interaction [31, 32, 33], such a distinct stiffness imposition may lead to an undesirable preference between the distal and proximal joints during walking. In contrast, noting that the multi-joint stiffness variations of a CDLE are dependent on its parameters, the current analysis show that an appropriate multi-joint stiffness characteristics between anisotropic to isotropic can be achieved. In general, a typical gait motion is achieved through a combination of hip and knee joint actuation, thus, for an effective gait rehabilitation paradigm using a CDLE, a desirable human–robot interaction can be attained through multi-joint stiffness tuning to promote a desired joint motion.

https://doi.org/10.1017/S0263574721000242 Published online by Cambridge University Press

6. Conclusion

The current work formulates the multi-joint stiffness as a measure to study the physical interaction between a human and CDLE. Theoretical analysis to articulate the effects of different system parameters, namely, cable tension, cable stiffness, cable routing, and motor positions, has been presented. The presented results show a significant role of cable routing, among other system parameters. In particular, a co-shared cable routing between the thigh and shank segments has the potential in producing a diverse multi-joint stiffness characteristic. The stiffness performance of two different cable routings has been validated experimentally to report a variation from being anisotropic to isotropic. In the context of movement training during a rehabilitation paradigm, the current analysis and results demonstrate the efficacy of performing architecture modulation for a CDLE in enabling the possibility of favorably tuning the human–robot interaction.

Acknowledgments. This work is partly supported from Inspire Faculty Award, DST, India, and from Early Career Research Award, SERB, India.

References

[1] S. K. Das, "Who steps stroke surveillance system: Feasibility in India," *Indian J. Med. Res.* **130**(4), 359–361 (2009).
[2] S. J. Olney and C. Richards, "Hemiparetic gait following stroke. Part I: Characteristics,"*Gait Posture* **4**(2), 136–148 (1996).
[3] S. K. Banala, S. H. Kim, S. K. Agrawal and J. P. Scholz, "Robot Assisted Gait Training with Active Leg Exoskeleton (Alex)," *2nd IEEE RAS & EMBS International Conference on Biomedical Robotics and Biomechatronics* (2008) pp. 653–658.
[4] T. George Hornby, D. H. Zemon and D. Campbell, "Robotic-assisted, bodyweight-supported treadmill training in individuals following motor incomplete spinal cord injury," *Phys. Therapy* **85**(1), 52–66 (2005).
[5] V. Vashista, D. Martelli and S. K. Agrawal, "Locomotor adaptation to an asymmetric force on the human pelvis directed along the right leg," *IEEE Trans. Neural Syst. Rehabil. Eng.* **24**(8), 872–881 (2015).
[6] M. E. Dohring and J. J. Daly, "Automatic synchronization of functional electrical stimulation and robotic assisted treadmill training," *IEEE Trans. Neural Syst. Rehabil. Eng.* **16**(3), 310–313 (2008).
[7] H. Thieme, "Enhanced gait-related improvements after therapist-versus roboticassisted locomotor training in subjects with chronic stroke: A randomized controlled study," *Physioscience* **4**(04), 195–196 (2008).
[8] D. Zanotto, P. Stegall and S. K. Agrawal, "Alex III: A Novel Robotic Platform with 12 DOFs for Human Gait Training," *2013 IEEE International Conference on Robotics and Automation* (IEEE, 2013) pp. 3914–3919.
[9] R. Riener, L. Lünenburger, I. C. Maier, G. Colombo and V. Dietz, "Locomotor training in subjects with sensori-motor deficits: an overview of the robotic gait orthosis lokomat," *J. Healthcare Eng.* **1**(2), 197–216 (2010).
[10] J. F. Veneman, R. Kruidhof, E. E. G. Hekman, R. Ekkelenkamp, E. H. F. Van Asseldonk and H. Van Der Kooij, "Design and evaluation of the lopes exoskeleton robot for interactive gait rehabilitation," *IEEE Trans. Neural Syst. Rehabil. Eng.* **15**(3), 379–386 (2007).
[11] P. Stegall, K. Winfree, D. Zanotto and S. K. Agrawal, "Rehabilitation exoskeleton design: Exploring the effect of the anterior lunge degree of freedom," *IEEE Trans. Rob.* **29**(4), 838–846 (2013).
[12] S. Srivastava, P.-C. Kao, S. H. Kim, P. Stegall, D. Zanotto, J. S. Higginson, S. K. Agrawal and J. P. Scholz, "Assist-as-needed robotaided gait training improves walking function in individuals following stroke." *IEEE Trans. Neural Syst. Rehabil. Eng.* **23**(6), 956–963 (2014).
[13] A. Alamdari and V. Krovi, "Design and analysis of a cable-driven articulated rehabilitation system for gait training," *J. Mech. Rob.* **8**(5), 051018 (2016).
[14] S. K. Banala, S. K. Agrawal, S. H. Kim and J. P. Scholz, "Novel gait adaptation and neuromotor training results using an active leg exoskeleton," *IEEE/ASME Trans. Mech.* **15**(2), 216–225 (2010).
[15] S. Jezernik, G. Colombo and M. Morari, "Automatic gait-pattern adaptation algorithms for rehabilitation with a 4-DOF robotic orthosis," *IEEE Trans. Rob. Autom.* **20**(3), 574–582 (2004).
[16] S. K. Banala, S. K. Agrawal, A. Fattah, V. Krishnamoorthy, W.-L. Hsu, J. Scholz and K. Rudolph, "Gravity-balancing leg orthosis and its performance evaluation.", *IEEE Trans. Rob.* **22**(6), 1228–1239 (2006).
[17] J. F. Veneman, R. Ekkelenkamp, R. Kruidhof, F. C. T. van der Helm and H. van der Kooij, "A series elastic-and bowden-cable-based actuation system for use as torque actuator in exoskeleton-type robots", *Int. J. Rob. Res.* **25**(3), 261–281 (2006).
[18] D. Zanotto, T. Lenzi, P. Stegall and S. K. Agrawal, "Improving transparency of powered exoskeletons using force/torque sensors on the supporting cuffs," **In:** *IEEE 13th International Conference on Rehabilitation Robotics (ICORR)* (IEEE, 2013) pp. 1–6.
[19] K. Gui, H. Liu and D. Zhang, "A practical and adaptive method to achieve EMG-based torque estimation for a robotic exoskeleton," *IEEE/ASME Trans. Mech.* **24**(2), 483–494 (2019).

[20] Z. Li, Y. Yuan, L. Luo, W. Su, K. Zhao, C. Xu, J. Huang and M. Pi, "Hybrid brain/muscle signals powered wearable walking exoskeleton enhancing motor ability in climbing stairs activity," *IEEE Transactions on Medical Robotics and Bionics.* **1**(4), 218–227 (2019).
[21] X. Li, Y. Pan, G. Chen and H. Yu, "Adaptive human–robot interaction control for robots driven by series elastic actuators," *IEEE Transactions on Robotics*. **33**(1), 169–182 (2016).
[22] S. Kim and J. Bae, "Force-mode control of rotary series elastic actuators in a lower extremity exoskeleton using model-inverse time delay control," *IEEE/ASME Trans. Mech.* **22**(3), 1392–1400 (2017).
[23] T. Boaventura, L. Hammer and J. Buchli, "Interaction Force Estimation for Transparency Control on Wearable Robots Using a Kalman Filter," **In:** *Converging Clinical and Engineering Research on Neurorehabilitation II* (Springer, Cham, 2017) pp. 489–493.
[24] X. Jin, X. Cui and S. K. Agrawal, "Design of a Cable-Driven Active Leg Exoskeleton (C-Alex) and Gait Training Experiments with Human Subjects,", *2015 IEEE International Conference on Robotics and Automation (ICRA)* (IEEE, 2015) pp. 5578–5583.
[25] M. Wu, T. George Hornby, J. M. Landry, H. Roth and B. D. Schmit, "A cable-driven locomotor training system for restoration of gait in human SCI," *Gait Posture* **33**(2), 256–260 (2011).
[26] A. Badi, M. Saad, G. Gauthier and P. Archambault, "Inverse kinematics for a novel rehabilitation robot for lower limbs," **In:** *Cable-Driven Parallel Robots* (Springer, Cham, 2018) pp. 376–389.
[27] A. Ming and T. Higuchi, "Study of multiple degree-of-freedom positioning mechanism using wires (part1) - concept, design and control," *Int. J. Japan Soc. Precis. Eng.* **28**(2), 131–138 (1994).
[28] S. Rezazadeh and S. Behzadipour, "Workspace analysis of multibody cable-driven mechanisms," *J. Mech. Rob.* **3**(2), 021005 (2011).
[29] D. Cafolla, M. Russo and G. Carbone, "CUBE, a cable-driven device for limb rehabilitation," *J. Bionic Eng.* **16**(3), 492–502 (2019).
[30] X. Zhou, S.-k. Jun and V. Krovi, "Tension distribution shaping via reconfigurable attachment in planar mobile cable robots," *Robotica* **32**(2), 245–256 (2014).
[31] R. Shadmehr and F. A. Mussa-Ivaldi, "Adaptive representation of dynamics during learning of a motor task," *J. Neurosci.* **14**(5), 3208–3224 (1994).
[32] H. Lee and N. Hogan, "Time-varying ankle mechanical impedance during human locomotion," *IEEE Trans. Neural Syst. Rehabil. Eng.* **23**(5), 755–764 (2014).
[33] A. F. Azocar and E. J. Rouse, "Stiffness perception during active ankle and knee movement," *IEEE Trans. Biomed. Eng.* **64**(12), 2949–2956 (2017).
[34] D. A. Winter, *The Biomechanics and Motor Control of Human Gait: Normal, Elderly and Pathological* (University of Waterloo Press, 1991).
[35] N. S. S. Sanjeevi and V. Vashista, "On the Stiffness Analysis of a Cable Driven Leg Exoskeleton," *2017 International Conference on Rehabilitation Robotics (ICORR)* (IEEE, 2017) pp. 455–460.
[36] S.-R. Oh and S. K. Agrawal, "Cable suspended planar robots with redundant cables: Controllers with positive tensions.", *IEEE Trans. Rob.* **21**(3), 457–465 (2005).
[37] M. Gouttefarde, D. Daney and J.-P. Merlet, "Interval-analysis-based determination of the wrench-feasible workspace of parallel cable-driven robots," *IEEE Trans. Rob.* **27**(1), 1–13 (2011).
[38] P. H. Borgstrom, B. L. Jordan, G. S. Sukhatme, M. A. Batalin and W. J. Kaiser, "Rapid computation of optimally safe tension distributions for parallel cable-driven robots," *IEEE Trans. Rob.* **25**(6), 1271–1281 (2009).
[39] F. A. Mussa-Ivaldi, N. Hogan and E. Bizzi, "Neural, mechanical, and geometric factors subserving arm posture in humans," *J. Neurosci.* **5**(10), 2732–2743 (1985).
[40] R. Verhoeven, M. Hiller and S. Tadokoro, "Workspace, Stiffness, Singularities and Classification of Tendon-Driven Stewart Platforms," *6th International Symposium on Advances in Robot Kinematics Salzburg, Austria* (1998).
[41] S. H. Yeo, G. Yang and W. B. Lim, "Design and analysis of cable-driven manipulators with variable stiffness," *Mech. Mach. Theory* **69**, 230–244 (2013).
[42] N. S. S. Sanjeevi and V. Vashista, "Effect of Cable Co-Sharing on the Workspace of a Cable-Driven Serial Chain Manipulator," *Proceedings of the Advances in Robotics 2019* (2019) pp. 1–6.
[43] S. F. Chen and I. Kao, "Conservative congruence transformation for joint and Cartesian stiffness matrices of robotic hands and fingers," *Int. J. Rob. Res.* **19**(9), 835–847 (2000).

Cite this article: N.S.S. Sanjeevi and V. Vashista (2021). "Stiffness modulation of a cable-driven leg exoskeleton for effective human–robot interaction", Robotica **39**, 2172–2192. https://doi.org/10.1017/S0263574721000242